Single-point parallel disk correction for asymptotically nonlinear oscillatory shear

N. Ashwin Bharadwaj · Randy H. Ewoldt

Abstract We derive exact single-point corrections for parallel disk measurements of all four asymptotically nonlinear measures under strain-controlled oscillatory shear. In this regime, sometimes called medium-amplitude oscillatory shear (MAOS), the derivatives appearing in the general stress correction are constant over the range of interest. This enables an exact single-point correction of all four shear stress components and material functions in the asymptotically nonlinear regime. This greatly simplifies the data processing and allows convenient measurements of true nonlinear material functions with parallel disk geometries. We use a strain amplitude expansion for the stress response, introducing a general non-integer strain amplitude scaling for the leading order nonlinearity, $\sigma \sim \gamma^{\alpha}$, where typically $\alpha = 3$ has been assumed in the past. The stress corrections are a multiplicative amplification by a factor $f(\alpha) = \frac{\alpha+3}{4}$, shown for the first time for all four asymptotically nonlinear coefficients. Experimental measurements are presented for the four asymptotically nonlinear signals on an entangled polymer melt of cis-1,4-polyisoprene, using both parallel disk and cone fixtures. The polymer melt follows a cubic ($\alpha = 3$) strain amplitude scaling in the MAOS regime. The theoretical corrections indicate a 50 % amplification of the apparent signals measured with the parallel disk fixture. The corrected (amplified) signals match the measurements with the cone.

Keywords Parallel disk rheometry · Single point correction · Asymptotically nonlinear rheology · Large amplitude oscillatory shear · Uncertainty propagation in MAOS · MAOS

N. A. Bharadwaj · R. H. Ewoldt (✉)
Department of Mechanical Science and Engineering,
University of Illinois at Urbana-Champaign,
Urbana, IL 61801, USA
e-mail: ewoldt@illinois.edu

Introduction

Parallel disk rotational rheometry has several advantages over a cone-plate setup. A plate-plate combination allows an adjustable gap height, a feature useful for loading stiff viscoelastic samples and irreversible gels prone to compressional fracture in the confines of a cone-plate setup. Additionally, the homogeneous gap in a parallel disk setup can ensure the material satisfies the continuum assumption at all radial locations, whereas a cone-plate geometry has a small truncated center point gap typically on the order of tens of micrometers, which risks violation of the continuum hypothesis for some structured materials. A parallel disk geometry is indispensable for such materials, including fiber-filled polymers (Férec et al. 2008), cross-linked gel networks (Ng et al. 2011), biopolymer networks (Fahimi et al. 2014), particle suspensions (McMullan and Wagner 2009; Ewoldt et al. 2009) and emulsions (Yoshimura and Prudhomme 1987).

Despite the advantages, a parallel disk fixture suffers from a major drawback: it imposes a radially inhomogeneous strain field that results in a radially inhomogeneous stress field. Thus, the calculation of true (edge) shear stress from the total torque is not always direct. An apparent edge stress can still be defined by a linear mapping to the total torque (details in section "Theory"), but this simplest calculation gives incorrect "apparent" nonlinear properties for the parallel-disk geometry. Figure 1 shows the measurement discrepancy between cone-plate and the apparent parallel-disk measurements in large-amplitude oscillatory shear (LAOS) (experimental details in section "Experiments"). In Fig. 1, and in general, apparent parallel disk measurements in LAOS tend to soften the nonlinearities, smoothing out the linear-to-nonlinear transition, and apparent nonlinear measures therefore have lower magnitudes with parallel

Fig. 1 Amplitude sweeps on cis-1,4-polyisoprene at $\omega = 1$ rad/s. (**a**), (**b**) Apparent nonlinear moduli from parallel disk measurements (squares) exhibit weaker nonlinearities compared to the true moduli from cone-plate measurements (triangles). (**c**), (**d**) A_3 and B_3 are *apparent* stress coefficients defined by Eq. 8. Both show a γ_0^3 scaling in the MAOS regime, with cone stresses being 50 % larger. Open symbols represent negative values. The low-torque limit is calculated from $\sigma_{\min}$ in Eq. 30 using $T_{\min} = 0.05$ μNm
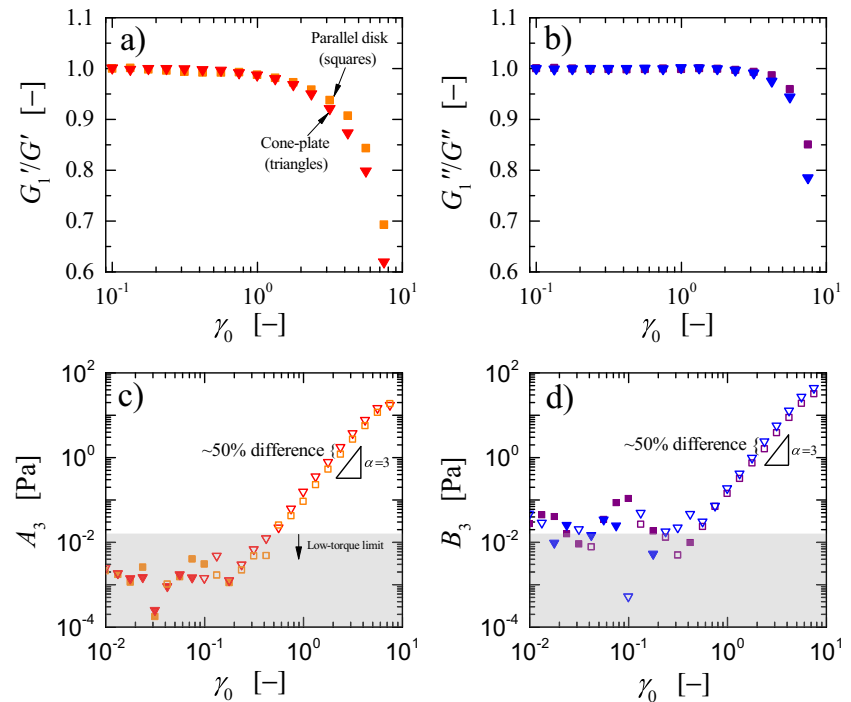
disks (Ewoldt et al. 2009; Stickel et al. 2013). This occurs because part of the sample will always be in the linear regime (due to smaller strains at sufficiently small radial position), in contrast to the nearly homogeneous strain field with a cone-plate geometry.

The true stress in parallel-disk measurements requires correction and involves partial derivatives of the torque response from one test to another. For steady flow measurements, corrections involve partial derivatives of the apparent steady flow stress with respect to the strain rate (Macosko 1994). The derivative calculation can be cumbersome with data processing and amplify experimental noise, so there have been various efforts to regularize (Yeow et al. 2004) or make single-point approximate corrections (Cross and Kaye 1987; Carvalho et al. 1994; Shaw and Liu 2006). The exact and approximate corrections are therefore useful for steady shear. Similar exact and approximate corrections have been used for time-dependent viscoelastic characterization protocols.

For strain-controlled large-amplitude oscillatory shear (LAOS) (a recent review is given by Hyun et al. (2011)), quantitative parallel disk corrections are available. Phan-Thien et al. (2000) identified a general correction that is always true; successful implementation requires calculation of partial derivatives with respect to strain amplitude, requiring multiple cycles of oscillation strain which is nontrivial. Ng et al. (2011) (see their supplemental information) gave additional details of the general LAOS correction, demonstrated implementation with real data of a gluten network, and discussed the implications of using (or not

using) such a correction. The numerical evaluation of the partial derivative invariably suffers from numerical noise. Fahimi et al. (2014) simplified the calculation by representing the apparent stress waveform as a Fourier series and computed the derivatives of the Fourier components rather than the derivatives of the raw data. These available corrections support LAOS experiments with parallel disk fixtures, but all require numerical differentiation of digital signals as a function of changing the input strain amplitude.

Here, we derive a general single-point correction (no numerical derivatives required) for parallel disk measurements of the four asymptotically nonlinear shear stress components (and material functions). The correction for the apparent shear stress is based on the key idea that the strain amplitude scaling is constant throughout this so-called medium-amplitude oscillatory shear (MAOS) regime.

Asymptotically-nonlinear rheological characterization is of interest for several reasons. Experimentally, measurements in fully nonlinear LAOS can suffer from experimental artifacts including nonideal flow conditions (Ravindranath and Wang 2008; Ravindranath et al. 2011), edge fracture (Mattes et al. 2008), and wall slip. These issues can be avoided by limiting the strains to an intermediate regime of medium-amplitude oscillatory shear (MAOS), also known as asymptotically (or intrinsically) nonlinear oscillatory shear (Ewoldt and Bharadwaj 2013). Even when correct LAOS measurements are experimentally obtainable, the theoretical understanding of LAOS characterization is challenging due to the high dimensionality of the response. Recent developments have enabled

a more systematic understanding in the low-dimensional asymptotically nonlinear regime (Hyun and Wilhelm 2009; Gurnon and Wagner 2012; Ewoldt and Bharadwaj 2013; Bharadwaj and Ewoldt 2014, 2015; Bozorgi and Underhill 2014).

Related corrections have been previously derived in the asymptotically-nonlinear regime, but only for the third-harmonic torque intensity (Wagner et al. 2011); they have been neither derived nor implemented for all *four* asymptotically nonlinear shear stress material functions (involving first-harmonic deviations and third-harmonic appearances). Furthermore, previous corrections have assumed a cubic strain amplitude scaling for the asymptotically nonlinear shear stress deviation from linearity (Wagner et al. 2011; Merger and Wilhelm 2014). Our theoretical results will acknowledge the possibility of a variable power expansion of strain amplitude scaling for the shear stress in MAOS, which may be required as suggested by some rheological constitutive models (Blackwell and Ewoldt 2014).

After deriving the theoretical corrections (section "Theory"), we demonstrate their use with experimental data (section "Experiments"). We show that the equations properly match experimental measurements taken with both cone-plate and parallel disk geometries on an entangled polymer melt. The correspondence is convincingly demonstrated with all four shear stress material functions over a range of frequencies (section "Experiments").

Theory

For unsteady strain-controlled shearing on a rotational rheometer, the control variable is a time-dependent angular displacement $\theta(t)$. The resulting strain of interest $\gamma(t)$ is calculated using a strain-conversion factor F_γ as

$$\gamma(t) = F_\gamma \theta(t) \tag{1}$$

where ideal conditions are assumed, such as no slip at the boundary, no secondary flow, and no viscoelastic waves – for a review of these experimental challenges see (Ewoldt et al. 2015). For a cone-plate setup with a linearly varying gap height $h(r)$, this conversion factor is a constant $F_{\gamma,c} = \frac{1}{h(r)} = \frac{1}{\tan\alpha}$, where α is the cone angle (Macosko 1994). The strain field in a cone-plate setup is thus radially homogeneous. On the contrary, a parallel disk setup with a constant gap height h results in a radially-dependent strain-conversion factor $F_{\gamma,p} = \frac{r}{h}$, and therefore a linearly varying heterogeneous strain field. It is useful to work with the rim shear strain $\gamma_R(t)$ at the edge of the disk having radius R

$$\gamma_R(t) = \frac{R}{h}\theta(t). \tag{2}$$

Practitioners typically use this variable for strain associated calculations (Macosko 1994).

The response to an imposed displacement (Eq. 1) is a torque $T(t)$ measured by the rheometer transducer. The measured torque can be directly mapped to an apparent shear stress using geometry-specific stress conversion factors

$$\sigma_c(t) = F_{\sigma,c} T(t), \tag{3}$$

$$\sigma_p(t) = F_{\sigma,p} T(t), \tag{4}$$

where the subscripts c and p stand for the cone and parallel disk fixtures respectively. The stresses are *apparent* as they are not measured directly, and their calculation from torque measurements requires assumptions which are sometimes violated (such as accurate sample volume loading, negligible viscoelastic waves in the sample, no surface tension forces, and no free surface effects – for a review of these experimental challenges see Ewoldt et al. (2015)). For a cone-plate setup with a homogeneous strain field distribution, the stress response is independent of the radial position, and it can be shown that $F_{\sigma,c} = \frac{3}{2\pi R^3}$. On the other hand, the simplest conversion for a parallel-disk fixture, Eq. 4, requires the assumption of a linear stress response to the imposed strain, resulting in an *apparent* plate shear stress (subscript p) at the rim

$$\sigma_p(t) = \frac{2}{\pi R^3}T(t). \tag{5}$$

Corrections to Eq. 5 have been provided by (Soskey and Winter 1984; Phan-Thien et al. 2000; Fahimi et al. 2014) with additional contributions from terms involving partial strain derivatives of the measured torque. These corrections resemble the Rabinowitsch correction in capillary rheometry (Macosko 1994).

In this work, we are interested specifically in oscillatory characterization. For sinusoidal strain excitations at amplitude γ_0 and frequency ω, the input shear strain waveform is conventionally given by (following Ewoldt (2013))

$$\gamma(t) = \gamma_0 \sin \omega t. \tag{6}$$

A linear stress response is elicited at small deformation amplitudes, and the protocol is called small amplitude oscillatory shear (SAOS). Parallel disk measurements in SAOS require no correction and Eq. 5 gives the *true* shear stress (if all other assumptions are valid). On the other extreme of large-amplitude oscillatory shear (LAOS), large deformations invoke a nonlinear stress response. In LAOS, parallel disk measurements involve a heterogeneous stress field for which Eq. 5 gives an apparent (and not a true) stress response.

In the same spirit as earlier proposed corrections, (Ng et al. 2011) provided corrections for the apparent edge shear

stress measured with a parallel disk fixture in LAOS. Their corrected stress (subscript p-corr) involves contributions from terms involving partial strain (amplitude) derivatives of the measured torque $T(t; \gamma_0, \omega)$ at a *fixed* cycle time t and fixed frequency ω

$$\sigma_{\text{p-corr}}(t; \gamma_0, \omega) = \frac{2}{\pi R^3} \left[\frac{3}{4} T(t; \gamma_0, \omega) + \frac{\gamma_0}{4} \frac{\partial T(t; \gamma_0, \omega)}{\partial \gamma_0} \right]. \quad (7)$$

Ng et al. (2011) implemented Eq. 7 to good effect on LAOS data from gluten gels, but this correction required multiple oscillations at different strains for a numerical evaluation of the partial derivative. Such numerical derivative calculations will always suffer from experimental noise. This can be avoided in the limit of asymptotically-nonlinear shear stress (or medium amplitude oscillatory shear (MAOS)), where the derivatives are typically known and are constants, thus allowing for single-point corrections for the apparent stress. We now derive the single point correction for asymptotically-nonlinear stress coefficients and material functions.

For an input shear strain given by Eq. 6, the resulting time-periodic, shear-symmetric and alternance-state shear stress waveform can be represented as a Fourier series expansion in the higher odd powers of the frequency ω (Philippoff 1966)

$$\sigma(t; \gamma_0, \omega) = \sum_{\substack{n=1 \\ odd}}^{\infty} A_n(\gamma_0, \omega) \sin n\omega t + B_n(\gamma_0, \omega) \cos n\omega t. \quad (8)$$

The coefficients $A_n(\gamma_0, \omega)$ and $B_n(\gamma_0, \omega)$ are directly measured in the experiment, since they are mapped from the torque, Eqs. 3–4. It is typical to report normalized Fourier moduli (Philippoff 1966; Onogi et al. 1970; Dealy and Wissbrun 1990) by scaling with the input strain amplitude γ_0

$$G'_n(\gamma_0, \omega) = \frac{A_n(\gamma_0, \omega)}{\gamma_0}, \quad (9)$$

$$G''_n(\gamma_0, \omega) = \frac{B_n(\gamma_0, \omega)}{\gamma_0}. \quad (10)$$

It is also possible to represent the shear stress as a power series expansion in increasing odd powers of the frequency ω (Onogi et al. 1970; Davis and Macosko 1978; Gurnon and Wagner 2012)

$$\sigma(t; \gamma_0, \omega) = \left(A_1^{(1)}(\gamma_0, \omega) \sin \omega t + B_1^{(1)}(\gamma_0, \omega) \cos \omega t \right) +$$
$$\begin{pmatrix} A_1^{(3)}(\gamma_0, \omega) \sin \omega t + B_1^{(3)}(\gamma_0, \omega) \cos \omega t + \\ A_3^{(3)}(\gamma_0, \omega) \sin 3\omega t + B_3^{(3)}(\gamma_0, \omega) \cos 3\omega t \end{pmatrix} + \ldots \quad (11)$$

The expansion in Eq. 11 does not assume any particular strain or rate amplitude scaling and is a suitable generalized form of representation. One can rewrite Eq. 11 with

material functions by scaling with respect to the input strain-amplitude γ_0 (Onogi et al. 1970; Ewoldt and Bharadwaj 2013)

$$\sigma(t; \gamma_0, \omega) = \gamma_0 \left(G'(\omega) \sin \omega t + G''(\omega) \cos \omega t \right)$$
$$+ \gamma_0^{\alpha} \begin{pmatrix} [e_1](\omega) \sin \omega t + [v_1](\omega) \omega \cos \omega t \\ -[e_3](\omega) \sin 3\omega t + [v_3](\omega) \omega \cos 3\omega t \end{pmatrix}$$
$$+ \mathcal{O}\left(\gamma_0^{\beta} \right). \quad (12)$$

where the Chebyshev domain is used for interpreting $[e_1](\omega)$, $[v_1](\omega)$, $[e_3](\omega)$, $[v_3](\omega)$ (Ewoldt and Bharadwaj 2013). Equation 12 is a generalized form affording flexibility with the strain-amplitude scaling through exponents α and β, where $\beta > \alpha$. Odd integer powers are typically observed for the strain-amplitude (or strain-rate amplitude) scaling, $\alpha = 3$, $\beta = 5$ etc. (Onogi et al. 1970; Pearson and Rochefort 1982; Helfand and Pearson 1982; Fan and Bird 1984; Nam et al. 2008; Liu et al. 2009; Giacomin et al. 2011; Stickel et al. 2013; Gurnon and Wagner 2012; Ewoldt and Bharadwaj 2013; Bharadwaj and Ewoldt 2014, 2015), but we have encountered other possibilities. For some thixotropic models, even - harmonic strain amplitude scaling in the MAOS regime is observed, i.e. $\alpha = 2$ (Blackwell and Ewoldt 2014). We have also observed the potential for non-integer strain-amplitude scaling for some models, such as the Cross model (Cross 1965; Bird et al. 1987; Macosko 1994). Material functions can be defined from the framework in Eq. 12: the two linear material functions $G'(\omega)$ and $G''(\omega)$ at $\mathcal{O}(\gamma_0)$, followed by the four asymptotically nonlinear material functions $[e_1](\omega)$, $[v_1](\omega)$, $[e_3](\omega)$, and $[v_3](\omega)$ at $\mathcal{O}(\gamma_0^{\alpha})$ (Ewoldt and Bharadwaj 2013; Blackwell and Ewoldt 2014).

The experimentally determined stress coefficients in Eq. 8 can be related to the material functions in Eq. 12 as

$$A_1(\gamma_0, \omega) = G'(\omega) \gamma_0 + [e_1](\omega) \gamma_0^{\alpha} + \mathcal{O}\left(\gamma_0^{\beta} \right) \quad (13)$$

$$B_1(\gamma_0, \omega) = G''(\omega) \gamma_0 + [v_1](\omega) \omega \gamma_0^{\alpha} + \mathcal{O}\left(\gamma_0^{\beta} \right) \quad (14)$$

$$A_3(\gamma_0, \omega) = -[e_3](\omega) \gamma_0^{\alpha} + \mathcal{O}\left(\gamma_0^{\beta} \right) \quad (15)$$

$$B_3(\gamma_0, \omega) = [v_3](\omega) \omega \gamma_0^{\alpha} + \mathcal{O}\left(\gamma_0^{\beta} \right). \quad (16)$$

Material functions are defined in the limits of small strains (using Eqs. 13–16) and can be related to the Fourier

moduli in Eqs. 9–10 and the power series expansion coefficients in Eq. 11. The two linear material functions are defined as

$$G'(\omega) \equiv \lim_{\gamma_0 \to 0} \frac{A_1(\gamma_0, \omega)}{\gamma_0} = \frac{A_1^{(1)}(\gamma_0, \omega)}{\gamma_0}, \tag{17}$$

$$G''(\omega) \equiv \lim_{\gamma_0 \to 0} \frac{B_1(\gamma_0, \omega)}{\gamma_0} = \frac{B_1^{(1)}(\gamma_0, \omega)}{\gamma_0}, \tag{18}$$

and the four asymptotically nonlinear material functions are defined as

$$[e_1](\omega) \equiv \lim_{\gamma_0 \to 0} \frac{A_1(\gamma_0, \omega) - G'(\omega)}{\gamma_0^\alpha} = \frac{A_1^{(3)}(\gamma_0, \omega)}{\gamma_0^\alpha}, \tag{19}$$

$$[v_1](\omega) \equiv \lim_{\gamma_0 \to 0} \frac{B_1(\gamma_0, \omega) - G''(\omega)}{\omega \gamma_0^\alpha} = \frac{B_1^{(3)}(\gamma_0, \omega)}{\omega \gamma_0^\alpha}, \tag{20}$$

$$[e_3](\omega) \equiv \lim_{\gamma_0 \to 0} \frac{-A_3(\gamma_0, \omega)}{\gamma_0^\alpha} = \frac{-A_3^{(3)}(\gamma_0, \omega)}{\gamma_0^\alpha}, \tag{21}$$

$$[v_3](\omega) \equiv \lim_{\gamma_0 \to 0} \frac{B_3(\gamma_0, \omega)}{\omega \gamma_0^\alpha} = \frac{B_3^{(3)}(\gamma_0, \omega)}{\omega \gamma_0^\alpha}. \tag{22}$$

These material functions are based on the assumption of asymptotically nonlinear stress scaling. Single-point corrections can now be obtained for these material functions for measurements with a parallel disk fixture.

The framework in Eqs. 11–12 can be used to represent both the apparent and the true shear stress response. To relate the apparent to the real shear stress, we use Eq. 5 in Eq. 7 and obtain

$$\sigma_{\text{p-corr}}(t; \gamma_0, \omega) = \frac{3}{4} \sigma_{\text{p}}(t; \gamma_0, \omega) + \frac{\gamma_0}{4} \frac{\partial}{\partial \gamma_0} \sigma_{\text{p}}(t; \gamma_0, \omega), \tag{23}$$

where the right-hand side involving the apparent stress $\sigma_{\text{p}}(t; \gamma_0, \omega)$ can be expanded in the form of Eq. 11 involving apparent stress coefficients $A_{1,p}^{(3)}(\omega)$, $A_{3,p}^{(3)}(\omega)$, $B_{1,p}^{(3)}(\omega)$, and $B_{3,p}^{(3)}(\omega)$. Similarly, the left-hand side can expand $\sigma_{\text{p-corr}}(t; \gamma_0, \omega)$ in the form of Eq. 11 to involve the corrected stress coefficients (subscript p-corr). The operator $\partial/\partial\gamma_0$ acts on all terms of the expanded $\sigma_{\text{p}}(t; \gamma_0, \omega)$, and the resultant expression will have the $\sin\omega t$, $\sin 3\omega t$, $\cos\omega t$, and $\cos 3\omega t$ terms. One can then equate coefficients of the trigonometric terms on each side of the expanded Eq. 23. This obtains single-point corrections for all four

stress coefficients through the same multiplicative front factor $f(\alpha)$

$$
\begin{aligned}
A_{1,\text{p-corr}}^{(3)}(\omega) &= f(\alpha) \ A_{1,p}^{(3)}(\omega), \\
A_{3,\text{p-corr}}^{(3)}(\omega) &= f(\alpha) \ A_{3,p}^{(3)}(\omega), \\
B_{1,\text{p-corr}}^{(3)}(\omega) &= f(\alpha) \ B_{1,p}^{(3)}(\omega), \\
B_{3,\text{p-corr}}^{(3)}(\omega) &= f(\alpha) \ B_{3,p}^{(3)}(\omega).
\end{aligned}
\tag{24}
$$

where the multiplicative correction is

$$f(\alpha) = \frac{\alpha + 3}{4} \tag{25}$$

which depends on the asymptotic strain-amplitude scaling exponent α in the power series expansion in Eq. 11. For the typically observed case of $\alpha = 3$,

$$f(\alpha = 3) = \frac{3}{2} \tag{26}$$

indicating that a 50 % increase is required to correct all four asymptotically nonlinear apparent stress signals, i.e., the first-harmonic deviations and the third-harmonic appearances.

One can also find corrections for the material functions if the apparent stress $\sigma_{\text{p}}(t; \gamma_0, \omega)$ in Eq. 23 is expanded in the form of Eq. 12 with apparent material function coefficients $[e_1]_p(\omega)$, $[e_3]_p(\omega)$, $[v_1]_p(\omega)$, and $[v_3]_p(\omega)$. The corrected material functions have a similar form to Eq. 24,

$$
\begin{aligned}
[e_1]_{\text{p-corr}}(\omega) &= f(\alpha) \ [e_1]_p(\omega), \\
[e_3]_{\text{p-corr}}(\omega) &= f(\alpha) \ [e_3]_p(\omega), \\
[v_1]_{\text{p-corr}}(\omega) &= f(\alpha) \ [v_1]_p(\omega), \\
[v_3]_{\text{p-corr}}(\omega) &= f(\alpha) \ [v_3]_p(\omega).
\end{aligned}
\tag{27}
$$

where $f(\alpha)$ is given in Eq. 25.

Equations 24–27 are the main analytical results of this work. These single-point corrections for strain-controlled MAOS allow for a variable strain amplitude scaling α, which can be measured and which is by definition constant in the asymptotically-nonlinear regime. These corrections are general in that strong assumptions of a particular constitutive theory are not required. That is, the corrections apply for any viscoelastic fluid or viscoelastic solid that has a linear viscoelastic regime followed by $\mathcal{O}(\gamma_0^\alpha)$ effects to the shear stress.

A subset of our results can be compared to previously obtained theoretical and experimental results in the MAOS regime. Hyun and Wilhelm (2009) defined a lumped intrinsic coefficient Q_0 that has been shown to be related to the

decoupled stress coefficients of Eq. 11 through the relation (Hyun and Wilhelm 2009; Bharadwaj and Ewoldt 2014)

$$Q_0 = \frac{1}{\gamma_0^2} \frac{\sqrt{\left(A_3^{(3)}\right)^2 + \left(B_3^{(3)}\right)^2}}{\sqrt{\left(A_1^{(1)}\right)^2 + \left(B_1^{(1)}\right)^2}}. \tag{28}$$

Using our results, an apparent $Q_{0,p}$ measured with a parallel plate can be corrected by using Eq. 24 in Eq. 28, resulting in the true coefficient

$$Q_{0,\text{p-corr}} = f(\alpha) \, Q_{0,p} \tag{29}$$

where $f(\alpha) = \frac{\alpha+3}{4}$ as obtained in Eq. 25. The result in Eq. 29, for the typical case $\alpha = 3$ with $f(\alpha) = \frac{3}{2}$, matches the earlier obtained result of Wagner et al. (2011). There, the lumped third-harmonic parameter correction was implemented in MAOS experiments on monodisperse polymer melts (Wagner et al 2011; Merger and Wilhelm 2014). As yet, there has been no experimental use or verification of a parallel disk correction for *decomposed* third-harmonic asymptotic measures, let alone the acknowledgment of needing to measure and correct first-harmonic asymptotic nonlinearities. This is pursued in the following section.

Experiments

We now demonstrate experimentally the general correction of Eqs. 24–27 applied to all four shear stress material function in strain-controlled MAOS, across a range of frequencies. Measurements on cis-1,4-polyisoprene are conducted with both parallel disk and cone-plate fixtures. We will show that $\alpha = 3$ for all four asymptotically nonlinear signals of this material system, implement the theoretically predicted 50 % amplification for the four apparent stress signals with a parallel-disk setup, and show that they match the cone-plate measurements.

Material and methods

Experiments are performed on a linear, well-entangled homopolymer melt of cis-1,4-polyisoprene with a molecular weight of 54,000, as supplied by Kuraray America Corporation. This material has been shown by Bharadwaj and Ewoldt (2014) to exhibit all four shear nonlinearities in MAOS and is therefore a suitable material choice for our experiments here. Bharadwaj and Ewoldt (2014) studied the terminal asymptotically nonlinear regime, but we will expand upon that work with measurements beyond the terminal regime.

A separated motor transducer ARES-G2 rheometer (TA Instruments) is used for experiments. The polymer melt is subjected to oscillatory shear deformation using a 25-mm diameter cone with a 0.1 radian cone angle, and a 25-mm diameter parallel-disk fixture at a gap of 1 mm. All experiments were performed at 25 °C regulated by a Peltier system at the bottom plate. Near isothermal conditions were maintained with the use of heat break tools (both the cone and parallel-disk fixtures).

Experimental results

Linear viscoelasticity for the polymer melt is shown as a frequency sweep at $\gamma_0 = 1$ % (Fig. 2). Measurements with the cone (triangles) and parallel-disk (squares) fixtures overlap reasonably well over the entire range of frequency. The overlap shows consistency between the two measurement geometries and reinforces the idea that, in the linear viscoelastic regime, no corrections are needed for parallel-disk measurements using apparent stress in Eq. 5.

Low-frequency measurements are affected by the torque resolution of the instrument. The minimum resolvable modulus $G_{\min}$ is governed by a criterion involving the instrument torque resolution $T_{\min}$ (Bharadwaj and Ewoldt 2014)

$$G_{\min} = \frac{\sigma_{\min}}{\gamma_0} = \frac{F_\sigma T_{\min}}{\gamma_0} \tag{30}$$

where $F_\sigma = \frac{2}{\pi R^3}$ is the stress conversion factor for the parallel-disk geometry with radius R. We use the manufacturer specified low-torque limit $T_{\min} = 0.05\,\mu\text{Nm}$, calculate $G_{\min} \approx 1.6$ Pa, and show this limit in Fig. 2. The subdominant storage modulus $G'(\omega)$ is affected by this limit at low frequency.
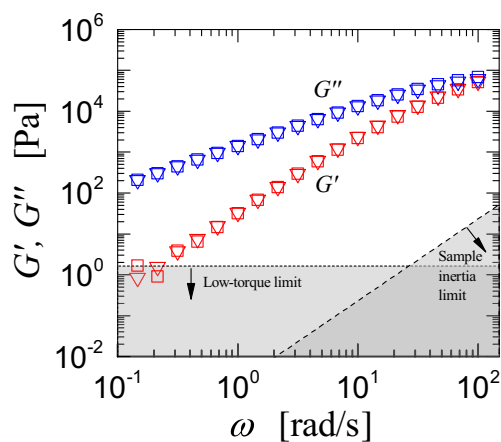
Fig. 2 Apparent linear viscoelastic measurements are identical for cone-plate (triangles) and parallel disk (squares), shown here through a frequency sweep at $\gamma_0 = 1$ %. Experimental limitations are shown for the low-torque limit (Eq. 30) and sample inertia which causes viscoelastic shear wave effects (Eq 31)

Fig. 3 The four apparent asymptotic nonlinearities for the parallel disk (squares) and cone-plate (triangles) geometries at $\omega = 1$ rad/s. Plateaus at small strain indicate the asymptotically nonlinear (MAOS) regime. Error bars are calculated using Eq. 32 from torques 100 times T_{noise} (identified from Fig. 4), those with first harmonics include error in fitting linear measures. (see Appendix for uncertainty propagation equations). Data is truncated to show the fit region
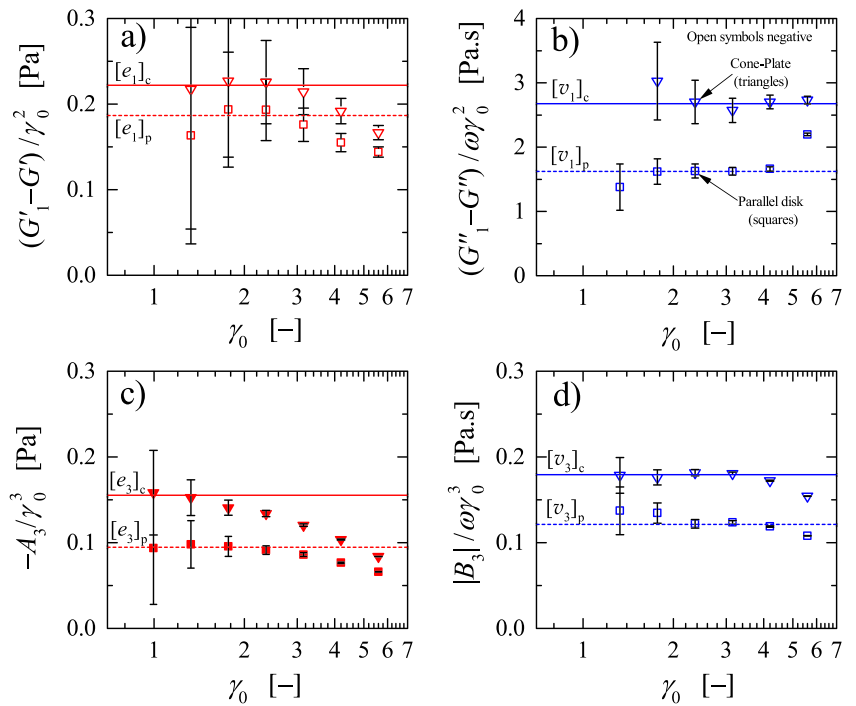
The experimental limit of sample inertia (viscoelastic shear waves) is avoided. At large frequency, viscoelastic shear wave propagation can violate the assumption of homogeneous deformation and result in sample inertia effects (Schrag 1977) (as a subset, the combination of viscous dissipation with fluid inertia also causes shear waves (Ding et al. 1999)). Using the criterion that the wavelength of the shear wave is at least 10 times the gap height h (Ewoldt et al. 2015), we estimate a sample inertia limit for the linear viscoelastic moduli, involving the density ρ and the phase angle δ,

$$G > \left(\frac{10}{2\pi}\right)^2 \cos^2(\delta/2) \rho h^2 \omega^2. \qquad (31)$$

Using the density of the polymer melt $\rho \approx 910$ kg/m³ (as reported by the supplier) and $\cos^2(\delta/2) \approx 1$, we identify the sample inertia limit in Fig. 2. Even at the highest frequency tested, the limit line is orders of magnitude below the data. This gives us confidence that our kinematics are negligibly influenced by transient shear wave effects.

Figure 1 shows that measurements of *nonlinear* apparent properties differ with geometry, probed experimentally by gradually increasing the strain amplitude at a fixed frequency. At $\omega = 1$ rad/s, Fig. 1a, b shows the strain amplitude dependence of the apparent, normalized first harmonic Fourier moduli (defined by Eqs. 9–10 with direct mapping to the total torque, Eqs. 3–4) measured with the cone (triangles) and parallel-disk (squares) fixtures. In the small-strain limit of linear viscoelasticity ($\gamma_0 \rightarrow 0$), measurements

with either geometry are identical. In the nonlinear regime, apparent parallel-disk measurements exhibit a weaker non-linear response compared to cone measurements and require corrections.

Apparent third-harmonic stress coefficients (defined by Eq. 8) are shown in Fig. 1c, d; the apparent plate non-linearities are smaller than the cone measurements. The experimental boundary defined by the minimum resolvable stress is shown for $T_{min} = 0.05$ μNm using σ_{min} in Eq. 30. In the limits of $\gamma_0 \rightarrow 0$, but above the torque noise limit, the asymptotically nonlinear strain amplitude scaling of stress coefficients is observed to be $A_3 \sim \gamma_0^3$ and $B_3 \sim \gamma_0^3$, as seen with both geometries. This indicates $\alpha = 3$ for this material in the MAOS regime (12), as typically assumed. For
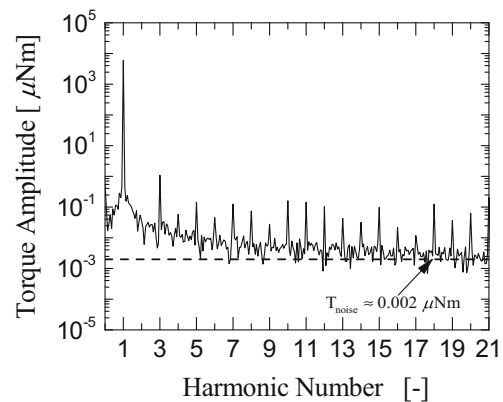
Fig. 4 The torque noise floor is identified from a power spectrum of the torque signal from oscillatory shear of cis-1,4-polyisoprene; shown here for $\omega = 1$ rad/s, $\gamma_0 = 125$ %, and 15 sampling cycles

Table 1 Ratio of cone to apparent parallel-disk nonlinearities calculated from fits to plateaus in Fig. 3. Theory predicts a ratio of $\frac{3}{2}$, Eqs. 26–27

Quantity	Value
$[e_1]_c/[e_1]_p$	1.2 ± 0.4
$[v_1]_c/[v_1]_p$	1.6 ± 0.1
$[e_3]_c/[e_3]_p$	1.6 ± 0.5
$[v_3]_c/[v_3]_p$	1.5 ± 0.1

$\alpha = 3$, the parallel disk correction factor is $f(\alpha = 3) = \frac{3}{2}$, from Eq. 25, which is a 50 % amplification of the apparent parallel-disk measurements. The 50 % increase of the apparent parallel plate third harmonics would then match the cone measurements in Fig. 1c, d.

Figure 3 identifies the asymptotically nonlinear material functions from the data in Fig. 1 by scaling the measured stress coefficients by γ_0^3. The cone nonlinear measurements (triangles) are always larger than the apparent parallel disk measurements (squares), as expected for LAOS. Plateaus in the limit of small strain identify the asymptotically nonlinear MAOS measures. For all four signals, a plateau region of constant asymptotic nonlinearity can be observed in the limits of small strain, but with an uncertainty associated with resolving the torque due to the torque noise ΔT_{noise}. Using the observed asymptotic scaling of γ_0^3 and ΔT_{noise}, we determine the uncertainty $\Delta \varepsilon$ in calculating normalized stress coefficients as

$$\Delta \varepsilon (\gamma_0) = \frac{F_\sigma \Delta T_{\text{noise}}}{\gamma_0^3}, \qquad (32)$$

where F_σ is the stress conversion factor. Error bars in Fig. 3a, d show this uncertainty $\Delta \varepsilon$, calculated from a torque 100 times the torque noise floor identified in Fig. 4, i.e., we use $\Delta T_{\text{noise}} = 100 T_{\text{noise}} = 0.2 \ \mu Nm$ in Eq. 32. The uncertainty bars with the first harmonic coefficients (Fig. 3a, b)

also include uncertainty in fitting the linear viscoelastic moduli G' and G'' from strain sweeps of the first-harmonic moduli G'_1 and G''_1. For a constant ΔT_{noise} in Eq. 32, the uncertainty in calculating the moduli is consistently smaller at larger strains, as shown in Fig. 3. These uncertainties are propagated to the fitting of a plateau (mean) asymptotic nonlinearity at small strains in Fig. 3a–d (see Appendix for details of uncertainty propagation).

To assess the plate correction, we evaluate the ratio of cone versus apparent plate measurements, e.g., $[e_3]_c/[e_3]_p$, and compare this to the theoretical prediction $[e_3]_{p\text{-corr}}/[e_3]_p = f(\alpha = 3) = \frac{3}{2}$, from Eq. 27. The measured ratios are shown in Table 1 along with the uncertainty in determining the ratio (see Appendix). Within expected measurement uncertainty, the ratios are consistent with the theoretically predicted value of $\frac{3}{2}$. The viscous nonlinearities are determined with better accuracy owing to larger viscous torques at this frequency, evident from smaller error bars with the viscous measures in Fig. 3b, d. The subdominant elastic contributions are resolved with less precision (larger error bars in Fig. 3a, c) and carry more uncertainty. The comparatively large uncertainty for the ratio of $[e_1]_c/[e_1]_p$ can be attributed to the difficulty in resolving the asymptotically nonlinear contribution from the subdominant first-harmonic elastic modulus G'_1 at this frequency. This asymptotically-nonlinear plateau fitting procedure can be repeated for a range of frequencies to generate a frequency-dependent asymptotic nonlinear fingerprint.

The frequency-dependent asymptotic nonlinear fingerprints are shown in Fig. 5 for the cone (triangles) and the parallel-disk (squares) geometries. The third harmonics are a pure nonlinearity; their measurements require that they are above the noise floor, in contrast to the first-harmonic nonlinearities that require subtraction of two large numbers G'_1 and G'. Thus, the third-harmonic intrinsic nonlinearities carry less uncertainty, and for clarity, we show only the third-harmonic nonlinearities in Fig. 5 (the error

Fig. 5 Parallel disk data are shifted up by an exact single-point correction factor for asymptotic nonlinearities (Eq. 27). Experimental data for cis-1,4-polyisoprene melt confirms agreement between cone-plate and corrected parallel disk measurements
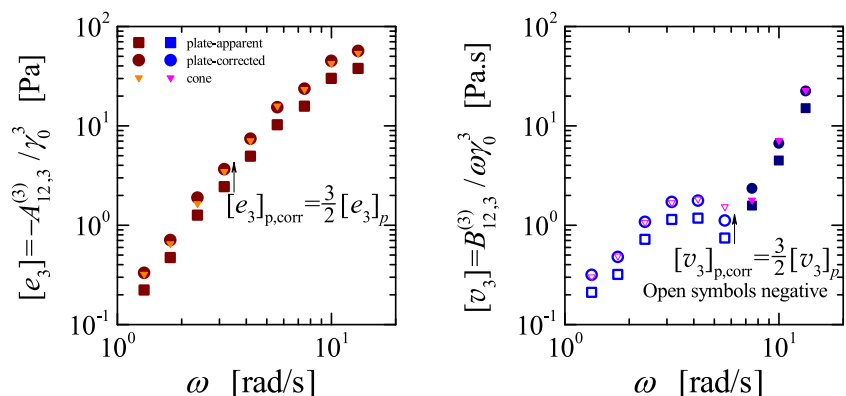
bars are less than or equal to the symbol size). For the frequencies considered, the apparent nonlinearities measured with the parallel disk fixture are smaller than the true nonlinearities reported with a cone (as mentioned, this is always expected for LAOS with parallel disks (Ewoldt et al. 2009)). Using the theoretically predicted shift factor $f(\alpha) = \frac{3}{2}$ in Eq. 27, the apparent parallel-disk non-linearities are amplified to match the cone measurements (circles matching triangles in Fig. 5). Mismatches occur at the location of a sign change in $[v_3]$, where the associated torque magnitude is small and difficult to resolve from noise.

Conclusions

A single-point correction is derived and experimentally demonstrated for parallel disk measurements in strain-controlled asymptotically-nonlinear oscillatory shear. This is an exact correction, not an approximation. Unlike previous corrections that have been shown only for the third-harmonic intensity, the corrections derived here apply to all four shear stress nonlinearities in the asymptotically nonlinear MAOS regime, i.e., the appearance of third harmonics *and* the deviation of first harmonics from linear viscoelastic moduli.

The corrections derived here allow for the possibility of non-cubic strain amplitude appearance of intrinsic nonlinearities. By assuming a general strain amplitude scaling α, each of the four apparent asymptotically nonlinear stress coefficients require a multiplicative correction factor $f(\alpha) = \frac{\alpha+3}{4}$, where typically $f(\alpha=3) = \frac{3}{2}$. This correction is universal in that strong assumptions of a particular constitutive theory are not required. That is, the correction applies for any viscoelastic fluid or viscoelastic solid that has a linear viscoelastic regime followed by $\mathcal{O}\left(\gamma_0^\alpha\right)$ effects to the shear stress.

Theoretical predictions are validated with strain-controlled MAOS experiments on an entangled linear polymer melt of cis-1,4-polyisoprene, using both parallel disk and cone geometries. The polymer shows the typical strain amplitude scaling of $\alpha = 3$ in the MAOS regime, indicating $f(\alpha) = \frac{3}{2}$, a 50 % amplification of the apparent asymptotically nonlinear stress coefficients. After amplification, the corrected stress coefficients match the true stress coefficients measured with a cone-plate fixture.

The predictions here are restricted to strain-controlled oscillatory shear. There is growing interest in stress-controlled oscillations (Läuger and Stettin 2010; Dimitriou et al. 2013; de Souza Mendes et al. 2014). A theoretical framework exists for stress-controlled MAOS (Ewoldt and Bharadwaj 2013), although stress-controlled MAOS material functions have not yet been reported in the literature. We

expect parallel disk corrections for the stress-control protocol will also be useful and can be derived with an approach similar to that used here, but this is beyond the scope of the work here.

The corrections proposed here will facilitate asymptotically-nonlinear experiments with several material systems that benefit from the parallel disk geometry, since it facilitates sample loading, minimizes slip with roughened surfaces, and better maintains the continuum assumptions. This includes biopolymers, large-mesh gel networks, colloidal suspensions, foams, and dense emulsions. Experiments combining rheometry and visualization often use parallel disk geometries to facilitate simultaneous velocimetry, optical microscopy, confocal imaging, and light scattering experiments, and these experiments will also benefit from the single-point corrections described here.

Appendix: Uncertainty propagation

Assuming small uncertainties ΔG_n for a measured quantity G_n, a first-order Taylor expansion provides a reasonable approximation for uncertainties associated with a calculated parameter $y = y(G_1, G_2, ..., G_n)$. The uncertainty in calculating y in its own dimensions is then given by (Beckwith et al. 1993)

$$\Delta y = \sqrt{\left(\frac{\partial y}{\partial G_1}\Delta G_1\right)^2 + \left(\frac{\partial y}{\partial G_2}\Delta G_2\right)^2 + ... + \left(\frac{\partial y}{\partial G_N}\Delta G_N\right)^2}. \tag{A1}$$

For the case where the mean of the N data points of G_n is sought, the parameter y can be calculated as

$$y = \frac{\sum\limits_{n=1}^{N} G_n}{N}. \tag{A2}$$

The partial derivatives in Eq. A1 can be calculated as

$$\frac{\partial y}{\partial G_1} = \frac{\partial y}{\partial G_2} = \frac{\partial y}{\partial G_N} = \frac{1}{N} \tag{A3}$$

to give the uncertainty in determining the mean of quantities G_n with their own uncertainties ΔG_n

$$\Delta y = \frac{1}{N}\sqrt{(\Delta G_1)^2 + (\Delta G_2)^2 + ... + (\Delta G_N)^2}. \tag{A4}$$

The uncertainties in the four asymptotically nonlinear moduli for the cone and parallel disk are calculated using Eq. A4 and propagated to calculate their respective ratios.

For determining the uncertainties in evaluating the ratio of the cone measurements to the apparent plate measurements shown in Table 1, we start with

$$y = \frac{G_1}{G_2}, \tag{A5}$$

and evaluate the partial derivatives in Eq. A1 as

$$\frac{\partial y}{\partial G_1} = \frac{1}{G_2}, \tag{A6}$$

$$\frac{\partial y}{\partial G_2} = -\frac{G_1}{G_2^2}. \tag{A7}$$

Using Eqs. A6 and A7 in Eq. A1, we evaluate the uncertainty in calculating the ratio of the two quantities as

$$\Delta y = \sqrt{\left(\frac{1}{G_2}\Delta G_1\right)^2 + \left(-\frac{G_1}{G_2^2}\Delta G_2\right)^2}. \tag{A8}$$

References

Beckwith TG, Marangoni RD, Lienhard JH (1993) Mechanical measurements, 5th ed., Addison-Wesley, New York, p 82

Bharadwaj NA, Ewoldt RH (2014) The general low-frequency prediction for asymptotically nonlinear material functions in oscillatory shear. J Rheol 58:891–910

Bharadwaj NA, Ewoldt RH (2015) Constitutive models under medium-amplitude oscillatory shear (MAOS). J Rheol. In press

Bird RB, Armstrong RC, Hassager O (1987) Dynamics of polymeric liquids, vol. 1, 2nd edn. Fluid mechanics. Wiley, New York

Blackwell BC, Ewoldt RH (2014) A simple thixotropic-viscoelastic constitutive model produces unique signatures in large-amplitude oscillatory shear (LAOS). J Non-Newtonian Fluid Mech 208-209:27–41

Bozorgi Y, Underhill PT (2014) Large-amplitude oscillatory shear rheology of dilute active suspensions. Rheol Acta 53:899–909

Brunn P, Asoud H (2002) Analysis of shear rheometry of yield stress materials and apparent yield stress materials. Rheol Acta 41:524–531

Carvalho MS, Padmanabhan M, Macosko CW (1994) Single-point correction for parallel disks rheometry. J Rheol 38:1925–1936

Cross MM (1965) Rheology of non-Newtonian fluids: a new flow equation for pseudoplastic systems. J Colloid Sci 20:417–437

Cross MM, Kaye A (1987) Simple procedures for obtaining viscosity/shear rate data from a parallel disc viscometer. Polymer 28:435–440

Davis WM, Macosko CW (1978) Nonlinear Dynamic Mechanical Moduli for Polycarbonate and PMMA. J Rheol 22:53–71

Dealy JM, Wissbrun KF (1990) Melt rheology and its role in plastics processing : theory and applications. Van Nostrand Reinhold, New York

De Souza Mendes PR, Thompson RL, Alicke AA, Leite RT (2014) The quasilinear large-amplitude viscoelastic regime and its significance in the rheological characterization of soft matter. J Rheol 58:537–561

Dimitriou CJ, Ewoldt RH, McKinley GH (2013) Describing and prescribing the constitutive response of yield stress fluids using large amplitude oscillatory stress (LAOStress). J Rheol 57:27–70

Ding F, Giacomin JA, Bird BR, Kweon C-B (1999) Viscous dissipation with fluid inertia in oscillatory shear flow. J Non-Newtonian Fluid Mech 86:359–374

Ewoldt RH (2013) Defining nonlinear rheological material functions for oscillatory shear. J Rheol 57:177–195

Ewoldt RH, Bharadwaj NA (2013) Low-dimensional intrinsic material functions for nonlinear viscoelasticity. Rheol Acta 52:201–219

Ewoldt RH, Johnston MT, Caretta LM (2015) Experimental challenges of shear rheology: how to avoid bad data. In: Spagnolie S (ed) Complex fluids in biological systems, Biological and Medical Physics, Biomedical Engineering. Springer, Berlin, New York, pp 207–241

Ewoldt RH, Winter P, Maxey J, McKinley GH (2009) Large amplitude oscillatory shear of pseudoplastic and elastoviscoplastic materials. Rheol Acta 49:191–212

Fahimi Z, Broedersz CP, van Kempen THS, Florea D, Peters GWM, Wyss HM (2014) A new approach for calculating the true stress response from large amplitude oscillatory shear (LAOS) measurements using parallel plates. Rheol Acta 53:75–83

Fan X-J, Bird RB (1984) A kinetic theory for polymer melts VI. Calculation of additional material functions. J Non-Newtonian Fluid Mech 15:341–373

Férec J, Heuzey MC, Ausias G, Carreau PJ (2008) Rheological behavior of fiber-filled polymers under large amplitude oscillatory shear flow. J Non-Newtonian Fluid Mech 151:89–100

Giacomin AJ, Bird RB, Johnson LM, Mix AW (2011) Large-amplitude oscillatory shear flow from the corotational Maxwell model. J Non-Newtonian Fluid Mech 166:1081–1099

Gurnon AK, Wagner NJ (2012) Large amplitude oscillatory shear (LAOS) measurements to obtain constitutive equation model parameters: Giesekus model of banding and nonbanding wormlike micelles. J Rheol 56:333–351

Helfand E, Pearson DS (1982) Calculation of the nonlinear stress of polymers in oscillatory shear fields. J Polym Sci Polym Phys Ed 20:1249–1258

Hyun K, Wilhelm M (2009) Establishing a new mechanical nonlinear coefficient Q from FT-rheology: first investigation of entangled linear and comb polymer model systems. Macromolecules 42:411–422

Hyun K, Wilhelm M, Klein CO, Cho KS, Nam JG, Ahn KH, Lee SJ, Ewoldt RH, McKinley GH (2011) A review of nonlinear oscillatory shear tests: Analysis and application of large amplitude oscillatory shear (LAOS). Prog Polym Sci 36:1697–1753

Läuger J, Stettin H (2010) Differences between stress and strain control in the non-linear behavior of complex fluids. Rheol Acta 49:909–930

Liu J, Yu W, Zhou W, Zhou C (2009) Control on the topological structure of polyolefin elastomer by reactive processing. Polymer 50:547–552

Macosko CW (1994) Rheology principles, measurements and applications. Wiley-VCH, New York

Mattes KM, Vogt R, Friedrich C (2008) Analysis of the edge fracture process in oscillation for polystyrene melts. Rheol Acta 47:929–942

McMullan JM, Wagner NJ (2009) Directed self-assembly of suspensions by large amplitude oscillatory shear flow. J Rheol 53:575–588

Merger D, Wilhelm M (2014) Intrinsic nonlinearity from LAOStrain—experiments on various strain- and stress-controlled rheometers: a quantitative comparison. Rheol Acta 53:621–634

Nam JG, Hyun K, Ahn KH, Lee SJ (2008) Prediction of normal stresses under large amplitude oscillatory shear flow. J Non-Newtonian Fluid Mech 150:1–10

Ng TSK, McKinley GH, Ewoldt RH (2011) Large amplitude oscillatory shear flow of gluten dough: a model power-law gel. J Rheol 55:627–654

Onogi S, Masuda T, Matsumoto T (1970) Non-linear behavior of viscoelastic materials. I. Disperse systems of polystyrene solution and carbon black. J Rheol 14:275–294

Pearson DS, Rochefort WE (1982) Behavior of concentrated polystyrene solutions in large-amplitude oscillating shear fields. J Polym Sci Polym Phys Ed 20:83–98

Phan-Thien N, Newberry M, Tanner RI (2000) Non-linear oscillatory flow of a soft solid-like viscoelastic material. J Non-Newtonian Fluid Mech 92:67–80

Philippoff W (1966) Vibrational measurements with large amplitudes. Trans Soc Rheol 10:317–334

Ravindranath S, Wang S-Q (2008) Large amplitude oscillatory shear behavior of entangled polymer solutions: particle tracking velocimetric investigation. J Rheol 52:341–358

Ravindranath S, Wang S-Q, Olechnowicz M, Chavan VS, Quirk RP (2011) How polymeric solvents control shear inhomogeneity in large deformations of entangled polymer mixtures. Rheol Acta 50(2):97–105

Schrag JL (1977) Deviation of velocity gradient profiles from the "gap loading" and "surface loading" limits in dynamic simple shear experiments. J Rheol 21:399–413

Shaw M, Liu Z (2006) Single-point determination of nonlinear rheological data from parallel-plate torsional flow. Appl Rheol 16:70–79

Soskey PR, Winter HH (1984) Large step shear strain experiments with parallel-disk rotational rheometers. J Rheol 28:625–645

Stickel JJ, Knutsen JS, Liberatore MW (2013) Response of elasto-viscoplastic materials to large amplitude oscillatory shear flow in the parallel-plate and cylindrical-Couette geometries. J Rheol 57:1569–1596

Wagner MH, Rolon-Garrido VH, Hyun K, Wilhelm M (2011) Analysis of medium amplitude oscillatory shear data of entangled linear and model comb polymers. J Rheol 55:495–516

Yeow YL, Chandra D, Sardjono AA et al. (2004) A general method for obtaining shear stress and normal stress functions from parallel disk rheometry data. Rheol Acta 44:270–277

Yoshimura AS, Prudhomme RK (1987) Response of an elastic Bingham fluid to oscillatory shear. Rheol Acta 26:428–436